6804 *Biochemistry* **2010,** *49,* 6804–6811
DOI: 10.1021/bi100567j

BIOCHEMISTRY
including biophysical chemistry & molecular biology
Article

Hematin−Hematin Self-Association States Involved in the Formation and Reactivity of the Malaria Parasite Pigment, Hemozoin[†]

Nectarios Klonis,[‡,§,#] Ruben Dilanian,[§,∥,#] Eric Hanssen,[‡,§,△] Connie Darmanin,[§,⊥] Victor Streltsov,[§,⊥] Samantha Deed,[‡,§] Harry Quiney,[§,∥] and Leann Tilley*[,‡,§]

[‡]*La Trobe Institute of Molecular Science, La Trobe University, Melbourne 3086, Australia,* [§]*ARC Centre of Excellence for Coherent X-ray Science, and* [∥]*School of Physics, The University of Melbourne, Victoria 3010, Australia, and* [⊥]*CSIRO, Molecular and Health Technologies, Melbourne, Australia* [#]*These authors contributed equally to this work.* [△]*Current address: Bio21 Molecular Science and Biotechnology Institute, University of Melbourne, Parkville, Victoria 3010, Australia*

Received April 13, 2010; Revised Manuscript Received June 17, 2010

ABSTRACT: The malaria parasite pigment, hemozoin, is a crystal of ferriprotoporphyrin IX (FP-Fe(III)), a product of hemoglobin digestion. Hemozoin formation is essential for FP-Fe(III) detoxification in the parasite; it is the main target of quinoline antimalarials and can modulate immune and inflammation responses. To gain further insight into the likely mechanisms of crystal formation and hemozoin reactivity, we have reanalyzed the crystal structure data for β-hematin and solved the crystal structure of *Plasmodium falciparum* hemozoin. The analysis reveals that the structures are very similar and highlights two previously unexplored modes of FP-Fe(III) self-association involving $\pi-\pi$ interactions that may initiate crystal formation and help to stabilize the extended structure. Hemozoin can be considered to be a crystal composed of $\pi-\pi$ dimers stabilized by iron−carboxylate linkages. As a result, it is predicted that two surfaces of the crystal would consist of $\pi-\pi$ dimers with Fe(III) partly exposed to solvent and capable of undergoing redox reactions. Accordingly, we demonstrate that the crystal possesses both general peroxidase activity and the ability to cause lipid oxidation.

Plasmodium falciparum is the causative agent of the most severe form of malaria in humans. As part of its complex life cycle, the parasite invades, grows, and multiplies within the red blood cells (RBCs) of its host. The parasite engulfs packets of hemoglobin from the host cell cytoplasm using a cytostome and transports the hemoglobin to an acidic digestive vacuole (*1*, *2*). In this acidic environment the hemoglobin is digested by the action of a series of proteases (*3*, *4*), and the prosthetic group, heme (ferroprotoporphyrin IX, FP-Fe(II)[1]), is oxidized to hematin (ferriprotoporphyrin IX, FP-Fe(III)) before undergoing a process of biocrystalization to form the malaria pigment, hemozoin.

FP-Fe(III) is a toxic molecule that can catalyze oxidative damage to lipids and proteins (*5*−*7*). The generation of hemozoin enables the parasite to sequester the FP-Fe(III) into a less toxic form. Nonetheless, hemoglobin degradation and hemozoin production represent a critical vulnerability of the malaria parasite that is targeted by a number of antimalarial drug classes (*8*−*11*). For example, quinoline antimalarials, such as chloroquine, inhibit hemozoin formation by binding to free FP-Fe(III) or to the hemozoin crystal (*12*). The resulting accumulation of FP-Fe(III) is thought to eventually overwhelm the parasite's antioxidant defense mechanisms.

Various spectroscopic techniques have been used to characterize hemozoin (*13*−*17*). It appears to be chemically and spectroscopically identical to β-hematin, which is formed by heating FP-Fe(III) in concentrated acetic acid at 60 °C (*13*, *18*−*20*) or at physiological temperatures if a suitable lipid−water interface is provided (*21*). The structure of β-hematin has been studied using X-ray powder diffraction (*22*). These studies revealed a repeating array of FP-Fe(III) dimers with the ferric iron of each monomer ligated to the propionate group of its partner. These iron−carboxylate interactions are assumed to ablate the redox activity of FP-Fe(III) molecules within the crystal. The structural studies also revealed hydrogen-bonding interactions, involving the remaining propionate side chains, which link the dimers into a two-dimensional matrix. The interactions that stabilize the crystal in the third dimension have been less well described.

The structure of hemozoin has not been solved *de novo*, but the powder diffraction patterns of preparations of hemozoin from *P. falciparum* are known to be similar to those of β-hematin (*14*, *22*). By contrast, an extended X-ray absorption fine structure (EXAFS) analysis of the K-edge of Fe in hemozoin and β-hematin (*23*) revealed a large uncertainty in the position of the oxygen atoms and a large value of the Debye−Waller factor in hemozoin compared with β-hematin, which is indicative of disordering as well as low occupancy for this atom. These authors suggested that fewer oxygen−Fe bonds are formed in hemozoin and that the crystal packing is, as a consequence, less ordered.

It is currently not well understood how hemozoin formation occurs *in vivo*. Early studies indicated involvement of a protein catalyst (*24*), but it is now generally agreed that hemozoin

[†]This work was supported by the Australian Research Council and the National Health and Medical Research Council, Australia.

*To whom correspondence may be addressed. E-mail: L.Tilley@latrobe.edu.au. Tel: (+61)-3-94793185. Fax: (+61)-3-94792467.

[1]Abbreviations: EXAFS, extended X-ray absorption fine structure; FP-Fe(II), ferroprotoporphyrin IX; FP-Fe(III), ferriprotoporphyrin IX; ABTS, 2′-azinobis(3-ethylbenzothiazoline-6-sulfonic acid); XRD, X-ray diffraction.

 Published on Web 07/01/2010

formation is a spontaneous process that is catalyzed by the lipid environment (*25*−*27*). It has been assumed that the dimeric iron−propionate unit of β-hematin is the nucleating species in hemozoin formation (*28*). Such dimeric intermediates have not, however, been observed in solution, and acetate is known to be a weak coordinating ligand for FP-Fe(III) (*29*). Molecular dynamics simulations in aqueous conditions support this conclusion but also indicate that such linkages are favored in a nonpolar environment (*21*). More recently, it has been suggested that crystallization may be initiated by the formation of a $\pi-\pi$ stacked dimer that subsequently converts to the β-hematin dimeric unit (*28*).

Hemozoin has been generally assumed to be an inert product with no redox activity. However, a number of studies have indicated that hemozoin has immunomodulatory activity both *in vivo* and *ex vivo* when it is engulfed by macrophages and dendritic cells (*30*−*32*). Some studies suggest that lipid and DNA contaminants associated with crude hemozoin are responsible for its interactions with immune cells (*33*, *34*); however, other studies using purified hemozoin or synthetic β-hematin show that the pure crystals are capable of producing similar effects (*35*).

In this work we have purified hemozoin from *P. falciparum* and solved the crystal structure at a resolution of 2.4 Å using powder diffraction data. Our analysis of the structural units that comprise the crystal allow us to propose a new model for the formation of hemozoin involving $\pi-\pi$ dimers as the nucleation unit, leading to the prediction that the surface of the crystal contains accessible iron in the form of Fe(III) that can participate in redox reactions. In support of this model, it is demonstrated that highly purified hemozoin has a general peroxidase activity and is capable of catalyzing lipid peroxidation. These findings have implications for understanding the immunomodulatory effects of hemozoin and its interaction with antimalarial drugs.

EXPERIMENTAL PROCEDURES

Hemozoin Preparation and Peroxidase Assays. Parasites (3D7 strain) were continuously cultured using RBCs and pooled serum obtained from the Red Cross Transfusion Service, Melbourne, Australia (*36*). Hemozoin was prepared from Percoll-enriched *P. falciparum* (3D7 strain) infected RBC, washed with 2% SDS and 6 M urea, incubated with proteinase K, and thoroughly washed with water (*37*). Porcine hematin (FP-Fe(III); Sigma) stocks were prepared in 50 mM NaOH. The concentration of FP-Fe(III) units in hematin and hemozoin preparations was determined spectrophotometrically after dilution in 50 mM NaOH using an extinction coefficient of 46.4 mM^{-1} cm^{-1} at 384 nm for monomeric FP-Fe(III) (*38*).

The peroxidase activity of FP-Fe(III) and hemozoin was determined in the presence of 2.5 mM H_2O_2 and 0.5 mM substrate 2,2′-azinobis(3-ethylbenzothiazoline-6-sulfonic acid) (ABTS; Sigma) in 50 mM sodium acetate, pH 5.5. Samples were prepared in triplicate in microplate wells and incubated at 37 °C with constant shaking, and the absorbance was measured periodically at 417 nm. The ability of FP-Fe(III) and hemozoin to promote lipid peroxidation was measured using the fluorescently labeled fatty acid 4,4-difluoro-5-(4-phenyl-1,3-butadienyl)-4-bora-3a,4a-diaza-*s*-indacene-3-undecanoic acid (BODIPY 581/591-FA; Invitrogen). Assays were performed in triplicate with 0.75 μM BODIPY 581/591-FA in 100 mM sodium acetate buffer, pH 5.5, containing 0.1% Triton X-100 (w/w). Samples were incubated at 37 °C with constant shaking and centrifuged at 15000*g* for 5 min to sediment the hemozoin, and the supernatants were transferred to an opaque microplate. Red and green fluorescence was monitored using excitation/emission wavelengths of 480/520 and 570/610 nm, respectively. Absorption and fluorescence measurements were recorded using a SpectraMax M5 microplate reader (Molecular Devices).

Hemozoin Structural Analysis. X-ray diffraction data (XRD) of hemozoin were collected at the 3BM-1 Protein Crystallography beamline at the Australian Synchrotron. The sample was mounted on a cryoloop and frozen under liquid nitrogen. A synchrotron radiation energy of 12.96 keV (λ = 0.956655 Å) was selected using a primary, tunable, double-crystal Si (111) beamline monochromator. The diffraction pattern was detected using a charge-coupled device camera (CCD) containing a 2048 × 2048 array of 102.4 μm pixels placed 200 mm from the sample. A set of 72 two-dimensional images with a 30 s exposure time was collected and analyzed to create a radially averaged one-dimensional diffraction pattern.

The structure of hemozoin was refined using the *m*aximum entropy-based *p*attern *f*itting approach (MPF) (*39*), which is an iterative combination of the Rietveld refinement method and the maximum entropy method (see Supporting Information). The Rietveld refinement was performed using RIATAN-2000 (*40*), and MEM analyses were performed using PRIMA (*39*). The split pseudo-Voigt function of Toraya (1990) was used as a profile function for the Rietveld refinement. The background was represented by a composite function, involving an 11th-order Legendre polynomial multiplied by a set of numerical values obtained using the program PowderX (*41*). Coefficients for the analytical approximations to the atomic scattering factors for Fe, O, N, and C were taken from ref *42* and anomalous scattering factors from ref *43*. The unit cell parameters of hemozoin were determined using DICVOL (*44*) and were further refined by RIETAN-2000. The atomic structure and electron density maps were drawn using the 3D visualization system, VENUS (*44*). In the MPF analysis, we used diffraction data with angular scattering occurring in the range from 3.025° to 22.695°, corresponding to a resolution of 2.4 Å. The atomic positions of β-hematin (*22*) were used to provide an initial model for structure refinement.

RESULTS

Determination of the structure of hemozoin was performed by first refining the fractional coordinates of Fe by the Rietveld method, using rigid body constraints for all other atoms. The MPF method was then applied to obtain the three-dimensional electron density distribution of hemozoin. Fractional coordinates of all atoms were finally refined using strong nonlinear restraints: 41 for interatomic distances and 52 for bond angles, respectively. Table 1 lists the resulting lattice parameters and *R* factors. Figure 1a illustrates calculated, observed, and difference patterns plotted as functions of 2θ. The two-dimensional projection of the reconstructed electron density distribution appears as Figure 1b, and the refined crystal structure of hemozoin is shown as Figure 1c.

The resolution limit does not allow us to determine the positions of C and N atoms with high accuracy. The positions of the Fe atoms, nevertheless, appear as peaks of high electron density in Figure 1b, and the orientation of the FP-Fe(III) molecules is readily determined. The resulting structure of hemozoin is very similar, within the 2.4 Å resolution limit, to that reported for β-hematin (*22*). The FP-Fe(III) appears as a typical, pentacoordinate structure with the iron atom protruding out of the plane of the porphyrin ring. The two FP-Fe(III) units in the unit cell

Table 1: Unit Cell Dimensions and *R* Factors for Hemozoin[a]

space group	$P\bar{1}$
Z	2
a (Å)	12.187(2)
b (Å)	14.692(2)
c (Å)	8.030(1)
α (deg)	90.94(1)
β (deg)	96.99(1)
γ (deg)	96.81(1)
R_{wp} (%)	6.18
R_p (%)	4.51
R_B (%)	1.28
R_E (%)	4.85
$\gamma = R_{wp}/R_E$ (goodness of fit)	1.27

[a]Figures in parentheses indicate approximate error in the final quoted digit in each quantity.

stack parallel to the iron porphyrin ring with the characteristic reciprocal iron−propionate linkages. Figure 1b also illustrates the electron density distribution along the FP-Fe(III)−O−FP-Fe(III) connection. The O−Fe bonding appears to be more disordered within the crystal lattice of hemozoin, an observation that is in agreement with results of a previous EXAFS study (*23*).

Figure 2 shows the electron density maps of the hemozoin crystal along three different axes. The hemozoin crystal may be regarded as consisting of a series of sheets with a thickness of ~11.0 Å. The surfaces between the sheets are relatively flat, but there is some complementarity. The noncoordinating carboxylic acid groups from each hemozoin unit in the unit cell dimer (indicated in black in Figure 2, lower panel) form reciprocal hydrogen bonds with the corresponding groups from adjacent sheets, effectively cross-linking the sheet network. Significant FP-Fe(III)−FP-Fe(III) interactions involving the metalloporphyrin moiety occur only within a sheet.

In order to identify the distinct FP-Fe(III)−FP-Fe(III) interactions that occur in the hemozoin crystal, we first analyzed the configuration of the Fe atoms within an individual sheet. The Fe atoms form two-dimensional layers (sheets) separated by a unit cell translation along the [100] direction, corresponding to a graphite-like configuration. The hexagonal outline model superimposed in Figure 3a indicates that each Fe atom within a sheet is surrounded by six other Fe atoms lying within a distance of less than 10 Å (Figure 3b,c). Two of the FP-Fe(III) units, Fe_0-Fe_3 and Fe_0-Fe_6, which are indicated by asterisks in Figure 3a, are not involved in direct interactions within the central FP-Fe(III) unit. The structural relationship between the remaining four FP-Fe(III) units and the central FP-Fe(III) unit is illustrated in Figure 4a. Table 2 shows the critical coordination parameters for the FP-Fe(III)−FP-Fe(III) contacts in hemozoin. Three distinct types of FP-Fe(III)−FP-Fe(III) interactions can be identified, as detailed below.

One of the FP-Fe(III) interactions involves the two FP-Fe(III) units in the unit cell. This "β-hematin dimer", Fe_0-Fe_5, has previously been described in detail (*9*). We prefer to call it the metal−propionate (μ−Pr) dimer to emphasize the importance of the iron−propionate linkage in stabilizing the dimer. The symmetrical transformation from the central FP-Fe(III) unit $\{x, y, z\}$ to its dimer partner is $\{1 + \bar{x}, 1 + \bar{y}, 1 + \bar{z}\}$. The dimer displays inversion symmetry through the center of the unit cell. The two porphyrin rings are orientated with their coordinated faces opposed. The key interaction between the two FP-Fe(III) units is the reciprocal Fe−O linkage involving the iron and carboxylate groups. Of the three FP-Fe(III)−FP-Fe(III) interactions occurring in the crystal, this one exhibits significantly longer Fe−Fe distances between the two units (Figure 3b) with little spatial overlap between the porphyrin rings (Figure 4b). This suggests that van der Waal interactions and $\pi-\pi$ bonding do not contribute significantly to the stability of this dimer.

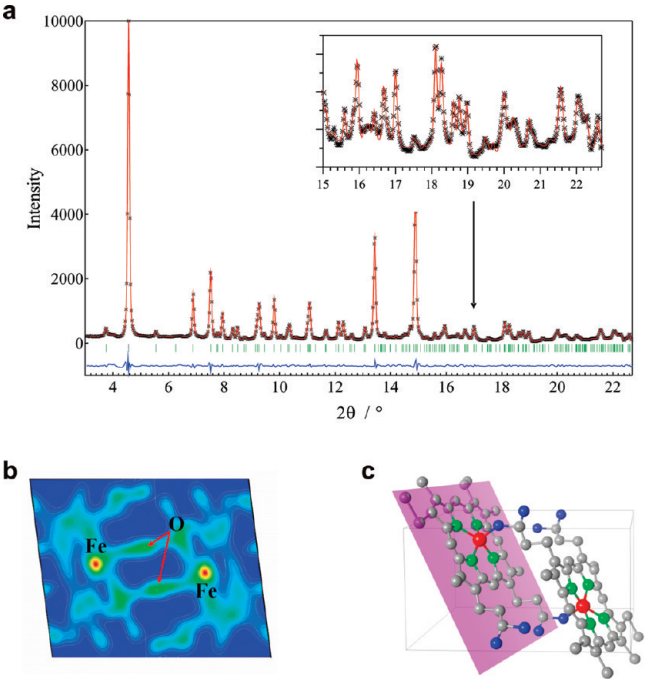

FIGURE 1: Determination of hemozoin structure from powder XRD data. (a) Powder XRD pattern from GSAS. The observed (crosses) and calculated (solid line) profiles are shown. The difference curve is shown below. Short vertical lines (green) below the profiles indicate peak positions of possible reflections. (b) Electron density (F_o) map of FP-Fe(III) (1σ level). (c) One unit cell of the crystal structure showing two molecules of FP-Fe(III).

A second, shorter FP-Fe(III)−FP-Fe(III) interaction can be described involving a FP-Fe(III) pair, which we designate as the $\pi-\pi$ dimer (Fe_0-Fe_2). In this dimer, the symmetrical transformation from the central FP-Fe(III) unit to its dimer partner is $\{1 + \bar{x}, \bar{y}, 2 + \bar{z}\}$. The second monomer is generated by the symmetry operations so that the two porphyrin rings are arranged with their noncoordinated faces mutually opposed. The Fe−Fe distances are shorter in this case (Figure 3b), and there is considerable spatial overlap of the two porphyrin rings involving both the porphyrin moieties and the vinyl groups, allowing π interactions between the units of the dimer (Figure 4c).

In a third FP-Fe(III)−FP-Fe(III) interaction, each FP-Fe(III) molecule contributes its vinyl and propionate ends to interactions with two different FP-Fe(III) molecules to form extended chains in a polymeric (P-type) interaction (Fe_0-Fe_1 and Fe_0-Fe_4). The symmetrical transformations from the central FP-Fe(III) unit to the two neighboring units are $\{x, y, 1 + z\}$ and $\{x, y, -1 + z\}$, respectively. In this case the metalloporphyrins have the same orientation but are translated along the (001) direction so that they are offset from each other. This association involves contacts between the noncoordinated face of the propionate end of one molecule and the coordinated face and vinyl region of the second molecule. The Fe−Fe distances are similar to those of the $\pi-\pi$ dimer (Figure 3b). There is no overlap between the porphyrin nuclei of the two FP-Fe(III) units although there is overlap between the vinyl group of one unit and the porphyrin group of the second unit contributing some $\pi-\pi$ interactions (Figure 4d,e).

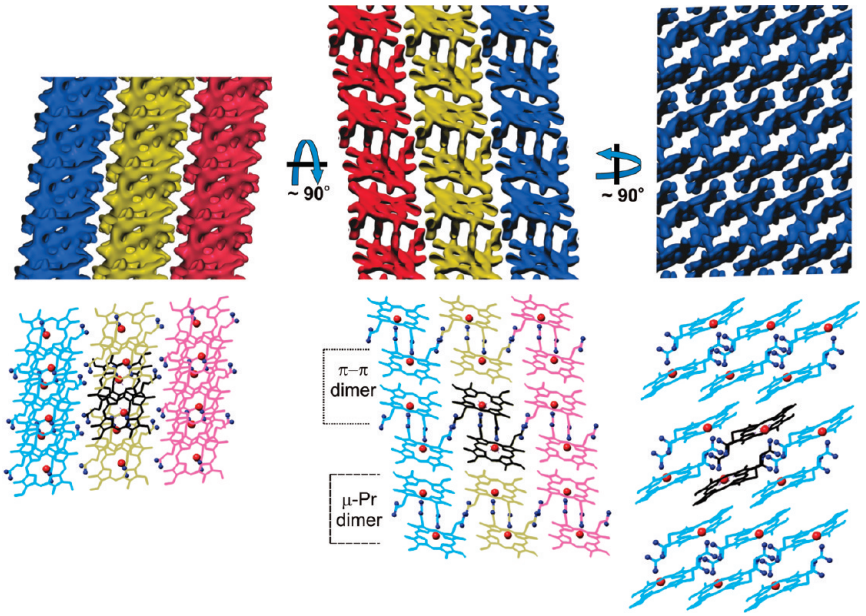

FIGURE 2: The hemozoin crystal is comprised of a series of sheets. The electron density map and crystal structure of hemozoin are shown along three different axes with 90° rotations of the crystal. Sheets of the crystal are colored blue, gold, and pink. The iron is represented as a red sphere, and the propionate oxygens are represented as dark blue balls in the wire-frame representations. One μ−Pr dimeric unit within the central sheet in each representation is colored black to illustrate its ability to form hydrogen bonds with sheets on either side. Each sheet can be considered to be made up of a series of μ−Pr dimers held together by π−π interactions or as a series of π−π dimers connected via μ−Pr linkages.

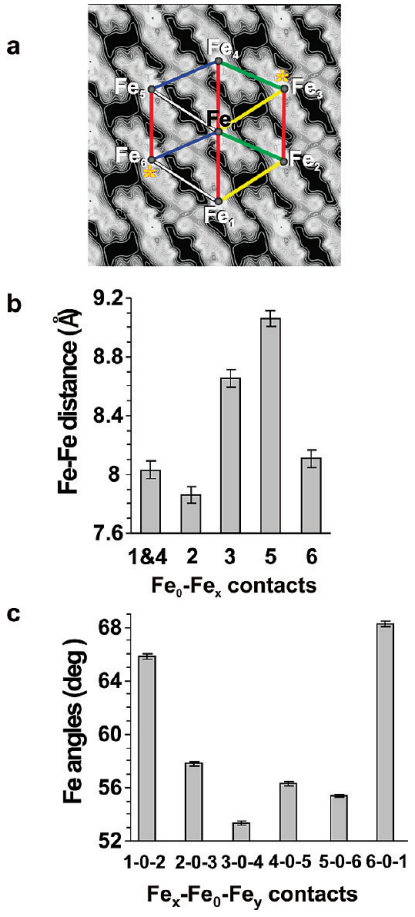

FIGURE 3: The geometrical configuration of Fe atoms within a sheet of the hemozoin crystal. (a) (100) projection of the normalized electron density of hemozoin showing that each Fe atom is surrounded by six Fe atoms in a distorted hexagonal configuration. The Fe_0−Fe_j distances and Fe_j−Fe_0−Fe_k angles are shown in (b) and (c), respectively.

This analysis suggests that hemozoin could be regarded as a crystal of π−π dimers rather than of μ−Pr dimers, in which case the crystal would support faces with iron at least partly exposed to the solvent that could participate in redox reactions. We examined the relative ability of FP-Fe(III) and freshly prepared, extensively washed hemozoin to act as general peroxidases using a colorimetric substrate. ABTS progressively reduces the oxidized hematin formed in the presence of hydrogen peroxide by one-electron reduction. The colored ABTS oxidation product can be followed spectrophotometrically. The analysis was performed at pH 5.5 to mimic the acidic conditions of the digestive vacuole. In the absence of hydrogen peroxide no oxidation of ABTS was observed with or without FP-Fe(III) or hemozoin over the time period examined (data not shown). Addition of hydrogen peroxide to ABTS caused a small level of ABTS oxidation (Figure 5a). This was significantly increased by the addition of submicromolar concentrations of FP-Fe(III) and was linear over the 4 h period of measurement (Figure 4a). Similar activity was observed when hemozoin was present at a concentration of 25 μM FP-Fe(III) units. This demonstrates that hemozoin possesses peroxidase activity although the level of activity per FP-Fe(III) unit is much lower than for free FP-Fe(III) (approximately 1.5%).

We also compared the ability of hemozoin and FP-Fe(III) to promote oxidation of the fluorescent lipid BODIPY 581/591-FA. The fluorescence emission maximum of the lipid probe is altered upon oxidation from red to green, permitting oxidation to be followed in a ratiometric analysis (*45*, *46*). Little or no oxidation of the fluorescent lipid occurs in the presence of the oxidizing agent *tert*-butyl hydroperoxide unless a redox catalyst is added (*45*) (Figure 5b). Upon addition of FP-Fe(III) or hemozoin a time-dependent increase in green emission and a decrease in red fluorescence are observed (Figure 5b). Hemozoin catalyzes the oxidation of BODIPY 581/591-FA with an efficiency per FP-Fe(III) unit that is approximately 1.5% of that of free FP-Fe(III).

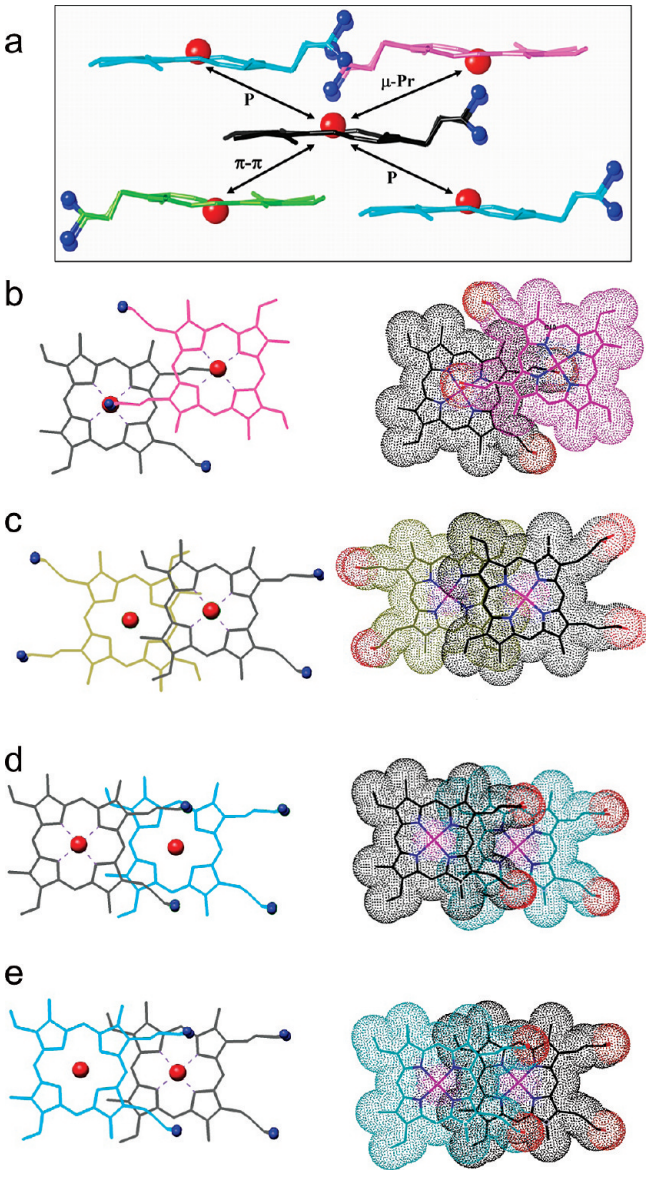

FIGURE 4: Metalloporphyrin interactions in the hemozoin crystal. (a) Each individual FP-Fe(III) unit (gray) is involved in a range of metalloporphyrin interactions with the surrounding FP-Fe(III) units. These involve μ−Pr (b, gray to pink), π−π (c, gray to green), and P-type (d and e, gray to blue) interactions. Each of these interactions is shown as wire-frame and space-filling representations. Note that the P-type interaction is asymmetric and is shown in two views. The iron is represented as a red sphere, and the propionate oxygens are represented as dark blue spheres.

DISCUSSION

We have employed a combination of the Rietveld refinement method and the maximum entropy method to refine the structure of hemozoin. This approach includes an iterative step of maximum entropy enhancement of the electron density. This helps to reduce any bias imparted on the solution by the choice of the initial structure, while resolving overlapping X-ray reflections through the refinement of an underlying structure model. This approach has been shown previously to give improved fit to one-dimensional diffraction data (*39*, *47*).

The analysis confirms that the structures of hemozoin and β-hematin are very similar, as suggested previously (*14*, *22*). There is nevertheless a clear indication of heterogeneity in the Fe−O coordination in hemozoin. This leads to a greater disorder

Table 2: Parameters for the FP-Fe(III)−FP-Fe(III) Contacts Observed in Hemozoin

FP-Fe(III) unit	Fe−Fe displacement[a] (Å)		porphyrin−porphyrin distance (Å)
	L	V	
μ−Pr	8.33(9)	3.74(9)	4.42(9)
P-type	6.75(9)	4.57(9)	4.42(9)
π−π	6.75(9)	4.19(9)	4.42(9)

[a]Relative displacement of iron atoms along the average plane (depicted in Figure 1c) through the porphyrin nucleus (L) and perpendicular to this plane (V).

in the crystal packing of hemozoin than in β-hematin, which may reflect differences in the mechanisms that lead to crystal formation in these materials. The β-hematin crystals that were used for XRD studies were formed by dehydrohalogenation of FP (*22*). This process may produce a highly homogeneous product. By contrast, hemozoin crystals are formed in a more heterogeneous environment. Hemozoin formation is initiated in the early ring stage of development in predigestive vacuoles (*2*, *48*). These early microcrystals may form in the absence of lipid catalysts given that lipid bodies accumulate in later stage parasites (*26*). The predigestive vacuoles fuse to form a mature digestive vacuole in the trophozoite stage of parasite growth (*2*). The hemozoin crystals increase in size during this stage of growth. The higher chemical disorder of the hemozoin crystal may reflect imperfections introduced during the different phases of the growth of the crystals. Alternatively, imperfections in the packing of FP-Fe(III) dimers at the hemozoin crystal surface could disrupt some of the μ−Pr interactions leading to a lower occupancy of the oxygen site in hemozoin compared with synthetic β-hematin.

Previous structural studies of hemozoin and β-hematin have assumed that they represent crystals of μ−Pr dimers and have considered π−π interactions only in the context of crystal packing. It has been assumed that the nucleating unit for the formation of hemozoin is a μ−Pr dimer. Our analysis of the structural units in the hemozoin (from this work) and of β-hematin (from a published structure (*22*)) reveals, however, the presence of three FP-Fe(III) self-association states. It is of interest to consider which of these is more likely to provide the nucleating unit. The μ−Pr shows no overlap between the porphyrin rings and is stabilized only by the iron−carboxylate linkage; this linkage would be destabilized in an aqueous environment (*29*). In contrast, the porphyrin moieties in the π−π and P-type structural units are more proximal and exhibit a much greater level of overlap, which would provide enhanced stability in an aqueous environment with solvated Fe atoms. Of these, the π−π dimers involve more substantive porphyrin ring overlap than the P-type interaction, and the π−π dimers are suggested to be the predominant state of FP-Fe(III) in solution (*49*, *50*).

Both π−π and P-type structural units are present in the crystal structures of other metalloporphyrins (*51*). Scheidt and Lee have classified the strength of π−π interactions in these crystals based on the lateral and mean plane separations of the porphyrin units and suggested that π−π dimers are not simply a consequence of crystal packing interactions. Similarly, aromatic ring pairs in proteins are separated by a preferential distance of between 4.5 and 7 Å (*52*). We propose, therefore, that hemozoin (and β-hematin) is a crystal of π−π dimers with P-type and μ−Pr interactions acting to stabilize the crystal structure. This departure from the currently accepted view of hemozoin as a crystal

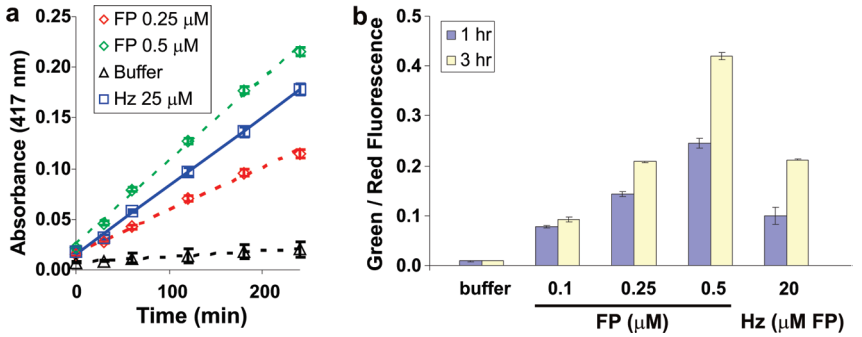

FIGURE 5: Redox activity of hemozoin. (a) Comparison of the peroxidase activity of FP-Fe(III) (at the indicated concentrations) and hemozoin (25 μM FP-Fe(III) units) using 0.5 mM ABTS in 2.5 mM H_2O_2 and 100 mM sodium acetate, pH 5.5, at 37 °C. (b) Comparison of the ability of FP-Fe(III) (at the indicated concentrations) and hemozoin (20 μM FP-Fe(III) units) to oxidize the fluorescent lipid BODIPY 581/591-FA (0.75 μM) in 100 mM sodium acetate buffer, pH 5.5, containing 0.1% Triton X-100 (w/w). Error bars correspond to the standard deviations of measurements performed in triplicate.

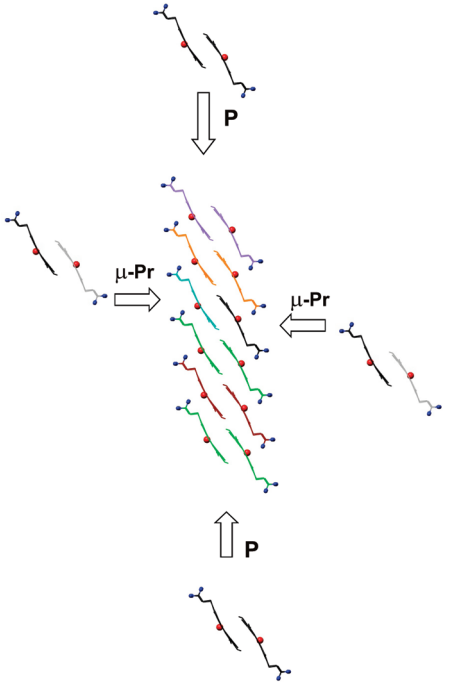

FIGURE 6: Proposed model for the formation of hemozoin. $\pi-\pi$ dimers form columnar aggregates via P-type interactions. Individual $\pi-\pi$ dimeric units are represented by the same color in the central columnar aggregate except for the initiating dimeric unit shown in blue and black. The columnar aggregate can be extended by the addition of more $\pi-\pi$ dimers (isolated dimers in black) via P-type interactions. The sheet can be extended in the second dimension by the formation of $\mu-$Pr linkages with other $\pi-\pi$ dimers (or between other columnar aggregates) represented by the isolated gray/black dimers. The result is the formation of a sheet made up of columns of $\pi-\pi$ dimers held together by $\mu-$Pr linkages. Note that the Fe atoms would be coordinated to hydroxide or water in an aqueous environment.

of $\mu-$Pr dimers has important implications for understanding its formation and properties.

A possible model for β-hematin/hemozoin crystal formation is illustrated in Figure 6. The nucleating species may comprise higher order associations of $\pi-\pi$ dimers into extended columns via P-type interactions. Such a species may represent the precipitated form of FP-Fe(III) which is favored under mildly acidic conditions. Under the conditions of the digestive vacuole (pH 5.5 (*53*)) the propionate groups will be partially neutralized and $\pi-\pi$ dimer formation will be favored, allowing higher order species to be formed (*50*). Extension of this oligomeric species into the second dimension, resulting in sheet formation, could occur through the formation of $\mu-$Pr linkages between the columnar oligomers. Crystal growth in the third dimension would then occur by association of the planar sheets, which are stabilized by van der Waals and reciprocal hydrogen-bonding interactions between the nonligated propionic acid groups on adjacent sheets; this would lock the sheets in place to form the regular crystal lattice of β-hematin/hemozoin.

A crystal of $\pi-\pi$ dimers constructed in the manner described above would possess different surface properties compared to a crystal composed of $\mu-$Pr dimers. In particular, $\pi-\pi$ dimers would be exposed on two surfaces of the crystal, which could influence the binding of antimalarial agents. For example, chloroquine and a number of other quinoline antimalarial drugs are thought to suppress parasite growth by inhibiting the detoxification of FP-Fe(III) (*8*, *24*, *54*, *55*). This is believed to occur by $\pi-\pi$ cofacial stacking directly to free FP-Fe(III) (*56*) and/or to hemozoin, thereby preventing further growth of the crystal (*8*). The binding of chloroquine to hemozoin has been modeled assuming that the $\mu-$Pr dimer forms part of the exposed surface (*57*). However, the crystal surfaces will be different if $\pi-\pi$ dimers form part of the exposed surface.

If hemozoin is a crystal comprised of $\pi-\pi$ dimers, it would be anticipated that the crystal will contain Fe(III) atoms that are at least partly exposed to solvent. These Fe(III) atoms may be able to interact with ligands and participate in redox reactions although steric effects may make them less reactive than free FP-Fe(III). We have demonstrated that hemozoin exhibits both a general peroxidase activity and the ability to catalyze lipid oxidation. The efficiency is approximately 1.5% of the activity of an equivalent amount of noncrystallized FP-Fe(III), which corresponds roughly to the proportion of Fe(III) atoms located close to the surface of a crystal with dimensions of 100 × 100 × 300−500 nm (*58*). Alternatively, the measured level of activity may reflect dissociation of $\pi-\pi$ dimer units bound by relatively weak P-type interactions at the crystal surface. Indeed, the association/dissociation of these units may account for the relatively small size of both β-hematin and hemozoin crystals. In either case, the data indicate that hemozoin crystals are not completely inert to redox reactions.

Our finding that hemozoin has redox activity is consistent with previous studies showing that hemozoin can induce lipid peroxidation (*59*, *60*). The formation of lipid peroxidation products could also explain the finding that hemozoin has immunomodulatory activity when it is engulfed by macrophages and dendritic

cells (*30*−*32*). The present work provides insight as to how this activity of hemozoin might arise.

The ability of hemozoin to participate in redox reactions has positive and negative aspects for the malaria parasite. The additional peroxidase or catalase activity within the parasite digestive vacuole may have useful antioxidant defense functions, particularly in contributing to the detoxification of hydrogen peroxide produced by heme oxidation during hemoglobin digestion. This comes at the expense, however, of the ability to cause additional oxidative damage to important protein and lipid substrates. Interestingly, hemozoin in the digestive vacuole is surrounded by lipid nanospheres that are postulated to facilitate hemozoin crystallization (*26*, *61*). The lipid components are poor in unsaturated lipids (*61*), which may represent a strategy to limit hemozoin-induced oxidative damage.

In summary, we have characterized the different FP-Fe(III) interactions within hemozoin crystals. This work provides insights into the nature of hemozoin formation and has implications for hemozoin processing by macrophages and for the action of antimalarial drugs. An increased understanding of these processes may lead to the development of antimalarial compounds with increased activity against this important human pathogen.

ACKNOWLEDGMENT

We thank Ms. Shannon Kenny and staff at the Australian Synchrotron, Melbourne, Australia, for technical assistance and Dr. Zhonghou Cai, Advanced Photon Source, Argonne National Laboratory, Argonne, IL, for help with initial studies. We thank Dr. Jose Varghese, CSIRO, for useful discussions.

SUPPORTING INFORMATION AVAILABLE

Detailed description of the *m*aximum entropy-based *p*attern *f*itting approach (MPF) used to refine the structure of hemozoin. This material is available free of charge via the Internet at http://pubs.acs.org.

REFERENCES

1. Slomianny, C. (1990) Three-dimensional reconstruction of the feeding process of the malaria parasite. *Blood Cells 16*, 369–378.
2. Abu Bakar, N. A., Klonis, N., Hanssen, E., Chan, C., and Tilley, L. (2010) Digestive-vacuole genesis and endocytic processes in the early intraerythrocytic stages of *Plasmodium falciparum*. *J. Cell Sci. 123*, 441–450.
3. Rosenthal, P. J., and Meshnick, S. R. (1996) Hemoglobin catabolism and iron utilization by malaria parasites. *Mol. Biochem. Parasitol. 83*, 131–139.
4. Banerjee, R., Liu, J., Beatty, W., Pelosof, L., Klemba, M., and Goldberg, D. E. (2002) Four plasmepsins are active in the *Plasmodium falciparum* food vacuole, including a protease with an active-site histidine. *Proc. Natl. Acad. Sci. U.S.A. 99*, 990–995.
5. Becker, K., Tilley, L., Vennerstrom, J. L., Roberts, D., Rogerson, S., and Ginsburg, H. (2004) Oxidative stress in malaria parasite-infected erythrocytes: host-parasite interactions. *Int. J. Parasitol. 34*, 163–189.
6. Balla, J., Vercellotti, G. M., Jeney, V., Yachie, A., Varga, Z., Jacob, H. S., Eaton, J. W., and Balla, G. (2007) Heme, heme oxygenase, and ferritin: how the vascular endothelium survives (and dies) in an iron-rich environment. *Antioxid. Redox Signaling 9*, 2119–2137.
7. Kumar, S., and Bandyopadhyay, U. (2005) Free heme toxicity and its detoxification systems in human. *Toxicol. Lett. 157*, 175–188.
8. Sullivan, D. J. (2002) Theories on malarial pigment formation and quinoline action. *Int. J. Parasitol. 32*, 1645–1653.
9. Egan, T. J. (2001) Structure-function relationships in chloroquine and related 4-aminoquinoline antimalarials. *Mini. Rev. Med. Chem. 1*, 113–123.
10. Tilley, L., Loria, P., and Foley, M. (2001) Chloroquine and other quinoline antimalarials, in Antimalarial Chemotherapy (Rosenthal, P. J., Ed.) pp 87−122, Humana Press, Totowa, NJ.
11. Slater, A. F. (1993) Chloroquine: mechanism of drug action and resistance in *Plasmodium falciparum*. *Pharmacol. Ther. 57*, 203–235.
12. Hanscheid, T., Egan, T. J., and Grobusch, M. P. (2007) Haemozoin: from melatonin pigment to drug target, diagnostic tool, and immune modulator. *Lancet Infect. Dis. 7*, 675–685.
13. Slater, A. F., Swiggard, W. J., Orton, B. R., Flitter, W. D., Goldberg, D. E., Cerami, A., and Henderson, G. B. (1991) An iron-carboxylate bond links the heme units of malaria pigment. *Proc. Natl. Acad. Sci. U.S.A. 88*, 325–329.
14. Bohle, D. S., Dinnebier, R. E., Madsen, S. K., and Stephens, P. W. (1997) Characterization of the products of the heme detoxification pathway in malarial late trophozoites by X-ray diffraction. *J. Biol. Chem. 272*, 713–716.
15. Adams, P. A., Berman, P. A., Egan, T. J., Marsh, P. J., and Silver, J. (1996) The iron environment in heme and heme-antimalarial complexes of pharmacological interest. *J. Inorg. Biochem. 63*, 69–77.
16. Webster, G. T., Tilley, L., Deed, S., McNaughton, D., and Wood, B. R. (2008) Resonance Raman spectroscopy can detect structural changes in haemozoin (malaria pigment) following incubation with chloroquine in infected erythrocytes. *FEBS Lett. 582*, 1087–1092.
17. Bohle, D. S., Conklin, B. J., Cox, D., Madsen, S. K., Paulson, S., Stephens, P. W., and Yee, G. T. (1994) Structural and spectroscopic studies of β-hematin (the heme coordination polymer in malaria pigment). *Am. Chem. Soc. Symp. Ser. 572*, 497–515.
18. Fitch, C. D., and Kanjananggulpan, P. (1987) The state of ferriprotoporphyrin IX in malaria pigment. *J. Biol. Chem. 262*, 15552–15555.
19. Sienkiewicz, A., Krzystek, J., Vileno, B., Chatain, G., Kosar, A. J., Bohle, D. S., and Forro, L. (2006) Multi-frequency high-field EPR study of iron centers in malarial pigments. *J. Am. Chem. Soc. 128*, 4534–4535.
20. Wood, B. R., Langford, S. J., Cooke, B. M., Glenister, F. K., Lim, J., and McNaughton, D. (2003) Raman imaging of hemozoin within the food vacuole of *Plasmodium falciparum* trophozoites. *FEBS Lett. 554*, 247–252.
21. Egan, T. J., Chen, J. Y., de Villiers, K. A., Mabotha, T. E., Naidoo, K. J., Ncokazi, K. K., Langford, S. J., McNaughton, D., Pandiancherri, S., and Wood, B. R. (2006) Haemozoin (beta-haematin) biomineralization occurs by self-assembly near the lipid/water interface. *FEBS Lett. 580*, 5105–5110.
22. Pagola, S., Stephens, P. W., Bohle, D. S., Kosar, A. D., and Madsen, S. K. (2000) The structure of malaria pigment β-haematin. *Nature 404*, 307–310.
23. Walczak, M., Lawniczak-Jablonska, K., Sienkiewicz, A., Demchenko, I. N., Piskorska, E., Chatain, G., and Bohle, D. S. (2005) Local environment of iron in malarial pigment and its substitute β-hematin. *Nucl. Instrum. Methods Phys. Res., Sect. B 238*, 32–38.
24. Slater, A. F., and Cerami, A. (1992) Inhibition by chloroquine of a novel haem polymerase enzyme activity in malaria trophozoites. *Nature 355*, 167–169.
25. Bendrat, K., Berger, B. J., and Cerami, A. (1995) Haem polymerization in malaria. *Nature 378*, 138–139.
26. Jackson, K. E., Klonis, N., Ferguson, D. J. P., Adisa, A., Dogovski, C., and Tilley, L. (2004) Food vacuole-associated lipid bodies and heterogeneous lipid environments in the malaria parasite, *Plasmodium falciparum*. *Mol. Microbiol. 54*, 109–122.
27. Fitch, C. D., Cai, G. Z., Chen, Y. F., and Shoemaker, J. D. (1999) Involvement of lipids in ferriprotoporphyrin IX polymerization in malaria. *Biochim. Biophys. Acta 1454*, 31–37.
28. Egan, T. J. (2008) Haemozoin formation. *Mol. Biochem. Parasitol. 157*, 127–136.
29. Sadasivan, N., Eberspaecher, H. I., Fuchsman, W. H., and Caughey, W. S. (1969) Substituted deuteroporphyrins. VI. Ligand-exchange and dimerization reactions of deuterohemins. *Biochemistry 8*, 534–541.
30. Carney, C. K., Schrimpe, A. C., Halfpenny, K., Harry, R. S., Miller, C. M., Broncel, M., Sewell, S. L., Schaff, J. E., Deol, R., Carter, M. D., and Wright, D. W. (2006) The basis of the immunomodulatory activity of malaria pigment (hemozoin). *J. Biol. Inorg. Chem. 11*, 917–929.
31. Urban, B. C., and Todryk, S. (2006) Malaria pigment paralyzes dendritic cells. *J. Biol. 5*, 4.
32. Wagner, H. (2010) Hemozoin: malaria's "built-in" adjuvant and TLR9 agonist. *Cell Host Microbe 7*, 5–6.
33. Parroche, P., Lauw, F. N., Goutagny, N., Latz, E., Monks, B. G., Visintin, A., Halmen, K. A., Lamphier, M., Olivier, M., Bartholomeu, D. C., Gazzinelli, R. T., and Golenbock, D. T. (2007) Malaria hemozoin is immunologically inert but radically enhances innate responses by presenting malaria DNA to Toll-like receptor 9. *Proc. Natl. Acad. Sci. U.S.A. 104*, 1919–1924.
34. Arese, P., and Schwarzer, E. (1997) Malarial pigment (haemozoin): a very active "inert" substance. *Ann. Trop. Med. Parasitol. 91*, 501–516.

35. Jaramillo, M., Bellemare, M. J., Martel, C., Shio, M. T., Contreras, A. P., Godbout, M., Roger, M., Gaudreault, E., Gosselin, J., Bohle, D. S., and Olivier, M. (2009) Synthetic plasmodium-like hemozoin activates the immune response: a morphology−function study. *PLoS ONE 4*, e6957.
36. Kalkanidis, M., Klonis, N., Tilley, L., and Deady, L. W. (2002) Novel phenothiazine antimalarials: synthesis, antimalarial activity, and inhibition of the formation of β-haematin. *Biochem. Pharmacol. 63*, 833–842.
37. Chen, M. M., Shi, L., and Sullivan, D. J., Jr. (2001) *Haemoproteus* and *Schistosoma* synthesize heme polymers similar to *Plasmodium* hemozoin and beta-hematin. *Mol. Biochem. Parasitol. 113*, 1–8.
38. Brown, S. B., Dean, T. C., and Jones, P. (1970) Aggregation of ferrihaems. Dimerization and protolytic equilibria of protoferrihaem and deuteroferrihaem in aqueous solution. *Biochem. J. 117*, 733–739.
39. Izumi, F., and Dilanian, R. A. (2002) Structure refinement based on the maximum-entropy method from powder diffraction data. *Recent Res. Dev. Phys. 3*, 699–724.
40. Izumi, F., and Ikeda, T. (2000) A Rietveld analysis program RIETAN-98 and its applications to zeolites. *Mater. Sci. Forum 321−324*, 198–205.
41. Dong, C. (1999) PowderX: Windows-95-based program for powder X-ray diffraction data processing. *J. Appl. Crystallogr. 32*, 838–838.
42. Prince, E. E. (2006) Mathematical, physical and chemical tables. Online edition, International Tables for Crystallography, *Vol. C* (http://it.iucr.org/C/).
43. Kissel, L., and Pratt, R. H. (1990) Corrections to tabulated anomalous-scattering factors. *Acta Crystallogr. A 46*, 170–175.
44. Izumi, F., and Dilanian, R. A. (2005) VENUS: a 3D visualization system for crystal structures and electron/nuclear densities. *IUCr Newslett. 32*, 59–63 (http://homepage.mac.com/fujioizumi/visualization/VENUS.html).
45. Fu, Y., Klonis, N., Suarna, C., Maghzal, G. J., Stocker, R., and Tilley, L. (2009) A phosphatidylcholine-BODIPY 581/591 conjugate allows mapping of oxidative stress in *P. falciparum*-infected erythrocytes. *Cytometry A 75*, 390–404.
46. Drummen, G. P., van Liebergen, L. C., Op den Kamp, J. A., and Post, J. A. (2002) C11-BODIPY(581/591), an oxidation-sensitive fluorescent lipid peroxidation probe: (micro)spectroscopic characterization and validation of methodology. *Free Radical Biol. Med. 33*, 473–490.
47. Izumi, F., Kumazawa, S., Ikeda, T., Hu, W. Z., Yamamoto, A., and Oikawa, K. (2001) MEM-based structure refinement system REMEDY and its applications. *Mater. Sci. Forum 378−381*, 59–64.
48. Dluzewski, A. R., Ling, I. T., Hopkins, J. M., Grainger, M., Margos, G., Mitchell, G. H., Holder, A. A., and Bannister, L. H. (2008) Formation of the food vacuole in *Plasmodium falciparum*: a potential role for the 19 kDa fragment of merozoite surface protein 1 (MSP1(19)). *PLoS ONE 3*, e3085.
49. Egan, T. J. (2008) Recent advances in understanding the mechanism of hemozoin (malaria pigment) formation. *J. Inorg. Biochem. 102*, 1288–1299.
50. Crespo, M. D. P., Tilley, L., and Klonis, N. (2010) Solution behavior of hematin under acidic conditions and implications for its interactions with chloroquine. J. Biol. Inorg. Chem. (in press).
51. Scheidt, W. R., and Lee, Y. J. (1987) Recent advances in the stereochemistry of metallotetrapyrroles. *Struct. Bonding* (*Berlin*) *64*, 1–70.
52. Burley, S. K., and Petsko, G. A. (1985) Aromatic-aromatic interaction: a mechanism of protein structure stabilization. *Science 229*, 23–28.
53. Klonis, N., Tan, O., Jackson, K., Goldberg, D., Klemba, M., and Tilley, L. (2007) Evaluation of pH during cytostomal endocytosis and vacuolar catabolism of hemoglobin in *Plasmodium falciparum*. *Biochem. J. 407*, 343−354.
54. Raynes, K., Foley, M., Tilley, L., and Deady, L. W. (1996) Novel bisquinoline antimalarials. Synthesis, antimalarial activity, and inhibition of haem polymerisation. *Biochem. Pharmacol. 52*, 551–559.
55. Dorn, A., Stoffel, R., Matile, H., Bubendorf, A., and Ridley, R. G. (1995) Malarial haemozoin/beta-haematin supports haem polymerization in the absence of protein. *Nature 374*, 269–271.
56. Vippagunta, S. R., Dorn, A., Matile, H., Bhattacharjee, A. K., Karle, J. M., Ellis, W. Y., Ridley, R. G., and Vennerstrom, J. L. (1999) Structural specificity of chloroquine-hematin binding related to inhibition of hematin polymerization and parasite growth. *J. Med. Chem. 42*, 4630–4639.
57. Buller, R., Peterson, M. L., Almarsson, O., and Leiserowitz, L. (2002) Quinoline binding site on malaria pigment crystal: a rational pathway for antimalaria drug design. *Cryst. Growth Des. 2*, 553–562.
58. Noland, G. S., Briones, N., and Sullivan, D. J., Jr. (2003) The shape and size of hemozoin crystals distinguishes diverse Plasmodium species. *Mol. Biochem. Parasitol. 130*, 91–99.
59. Schwarzer, E., Bellomo, G., Giribaldi, G., Ulliers, D., and Arese, P. (2001) Phagocytosis of malarial pigment haemozoin by human monocytes: a confocal microscopy study. *Parasitology 123*, 125–131.
60. Green, M. D., Xiao, L., and Lal, A. A. (1996) Formation of hydroxyeicosatetraenoic acids from hemozoin-catalyzed oxidation of arachidonic acid. *Mol. Biochem. Parasitol. 83*, 183–188.
61. Pisciotta, J. M., Coppens, I., Tripathi, A. K., Scholl, P. F., Shuman, J., Bajad, S., Shulaev, V., and Sullivan, D. J., Jr. (2007) The role of neutral lipid nanospheres in *Plasmodium falciparum* haem crystallization. *Biochem. J. 402*, 197–204.